ACS APPLIED MATERIALS & INTERFACES

Research Article

www.acsami.org

Conducting Polymer-Skinned Electroactive Materials of Lithium-Ion Batteries: Ready for Monocomponent Electrodes without Additional Binders and Conductive Agents

Ju-Myung Kim, Han-Saem Park, Jang-Hoon Park, Tae-Hee Kim, Hyun-Kon Song,* and Sang-Young Lee*

Department of Energy Engineering, School of Energy, Chemical Engineering, Ulsan National Institute of Science, Technology (UNIST), Ulsan 689-798, Korea

Supporting Information

ABSTRACT: Rapid growth of mobile and even wearable electronics is in pursuit of high-energy-density lithium-ion batteries. One simple and facile way to achieve this goal is the elimination of nonelectroactive components of electrodes such as binders and conductive agents. Here, we present a new concept of monocomponent electrodes comprising solely electroactive materials that are wrapped with an insignificant amount (less than 0.4 wt %) of conducting polymer (PEDOT:PSS or poly(3,4-ethylenedioxythiophene) doped with poly(styrenesulfonate)). The PEDOT:PSS as an ultraskinny surface layer on electroactive materials ($LiCoO_2$ (LCO) powders are chosen as a model system to explore feasibility of this new concept) successfully acts as a kind of binder as well as mixed (both electrically and ionically) conductive film, playing a key role in enabling the monocomponent electrode. The electric conductivity of the monocomponent LCO cathode is controlled by simply varying the PSS content and also the structural conformation (benzoid-favoring coil structure and quinoid-favoring linear or extended coil structure) of PEDOT in the PEDOT:PSS skin. Notably, a substantial increase in the mass-loading density of the LCO cathode is realized with the PEDOT:PSS skin without sacrificing electronic/ionic transport pathways. We envisage that the PEDOT:PSS-skinned electrode strategy opens a scalable and versatile route for making practically meaningful binder-/conductive agent-free (monocomponent) electrodes.

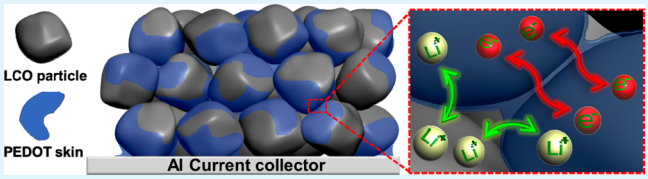

KEYWORDS: *binder/conductive agent free, conducting polymers, lithium-ion batteries, monocomponent electrodes, poly(3,4-ethylenedioxythiophene)*

INTRODUCTION

As a promising power source for rapidly growing industrial fields such as smart mobile electronics, electric vehicles, and grid-scale energy storage systems, advanced lithium-ion batteries (LIBs) affording high energy densities with reliable electrochemical performances are requested.[1−4] Most research efforts to address the challenging issues have been devoted to synthesis and structural manipulation of electroactive materials.[5−7] Conventional LIB electrodes consist of three components including active materials, binders, and conductive agents (carbon black) on current collectors (copper (Cu) or aluminum (Al) foils). From the viewpoint of pursuing high energy density, use of binders and conductive agents, which are not directly involved in faradaic reactions of LIBs, should be minimized to incorporate more active materials into a fixed volume of electrode. Also, introduction of the additional inactive components complicates electrode fabrication processes. Moreover, side reactions can be involved at the interface between the multicomponents and electrolyte.[6−9] To minimize the additional components, various approaches have been reported.[8−19] Use of conductive binders diminished the amount of conductive agents.[11−14] More extremely, active materials were attached directly to the electrode surface via hot-wire chemical vapor deposition (CVD)[15] or electrophoretic deposition.[16] However, previous works were based on sophisticated and practically inapplicable fabrication processes with nanostructured active materials. Therefore, a strategy that is compatible with readily available active materials as well as currently established manufacturing processes is required. A major objective of this work is to develop a facile and scalable fabrication strategy of not only binder-free but also conductive agent-free electrodes.

Herein, pseudomonocomponent electrodes (denoted concisely as monocomponent electrodes) are built of an active material wrapped with an insignificant amount of a conducting polymer. Neither additional binder nor conductive agent is introduced into the composite electrodes. $LiCoO_2$ (LCO) powders as the active material are coated ultrathinly and conformably with PEDOT:PSS (poly(3,4-ethylenedioxythiophene) doped with poly(styrenesulfonate)) as the conducting polymer. The PEDOT:PSS skin shows multifunctionality not only as a binder but also as a conductive agent, while its

Received: May 6, 2014
Accepted: July 2, 2014
Published: July 2, 2014

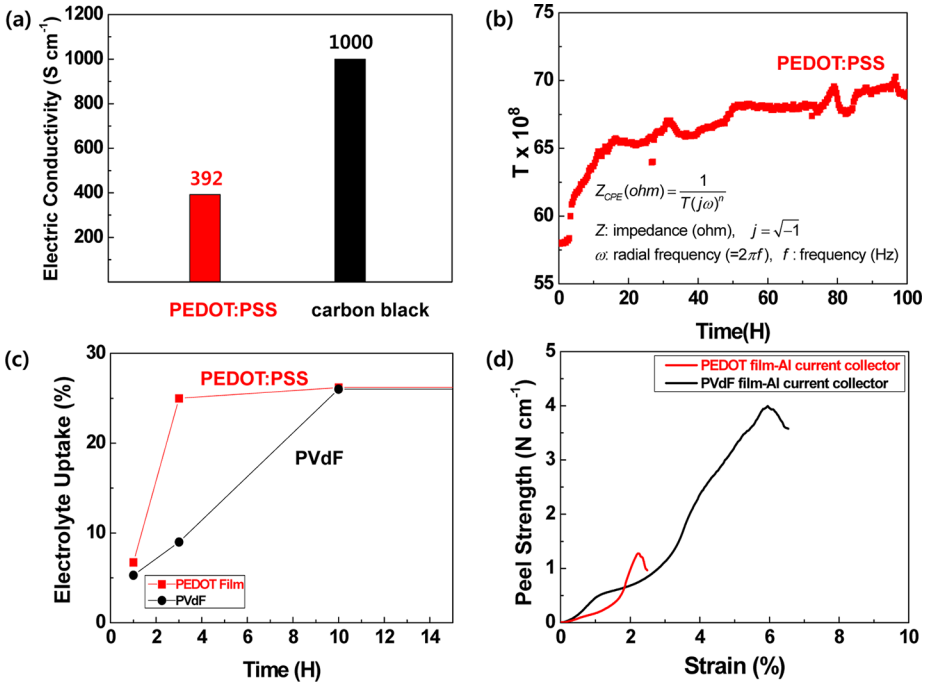

Figure 1. Physicochemical properties of PEDOT:PSS as a self-standing film. (a) Electric conductivity. (b) Wettability measured in situ by EIS. *T* is a measure of interfacial area between electrode and electrolyte. (c) Temporal change of electrolyte uptake. (d) Peel-off strength.

contribution to volume or mass is negligible. The PEDOT:PSS-skinned LCO (LCO@PEDOT:PSS) powders enable a scalable and versatile process of making binder-free and conductive agent-free (monocomponent) electrodes. Although conducting polymers have been used to enhance performances of LIBs,[20−23] additional binders or conductive agents were indispensably required in the previous works.

EXPERIMENTAL SECTION

LCO@PEDOT:PSS. One weight percent aqueous solutions of PEDOT:PSS (Clevios) with two different PSS contents (X_{PSS} [mol-based monomeric units of PSS per mole of PEDOT] = 3.3 and 7.8 for PH1000 and AI4083) were used for films or coating layers of benzoidal conformation. Five weight percent dimethyl sulfoxide (DMSO) was introduced to the solutions for developing quinoidal conformation of PEDOT:PSS. LCO powders (average particle size = 5 um; Umicore) were added to the PEDOT:PSS solutions diluted with deionized water at a weight ratio of 1:1. Suspensions were sonicated at room temperature for 30 min and then stirred at 80 °C for 24 h.

Electrodes. Conventional tricomponent electrodes were fabricated by coating Al foils with *N*-methyl-2-pyrrolidone (NMP)-based slurries of LCO/PVdF/carbon black (95:3:2 wt %). Monocomponent electrodes were obtained by coating the foils with aqueous slurries of only LCO@PEDOT:PSS. Coin cells of 2032 type were assembled by sandwiching a polyethylene separator (thickness = 20 um, Tonen) between a natural graphite anode and the cathode electrodes mentioned above (tricomponent or monocomponent). One molar $LiPF_6$ solutions of ethylene carbonate (EC)/dimethyl carbonate (DMC) (1/1 v/v, Soulbrain) were used as an electrolyte.

Electric Properties. Electric conductivities were measured using a four-point probe technique (CMT-SR1000N, Advanced Instrument Technology). Monocomponent slurries in water or tricomponent slurries in NMP were coated on glass substrates (1.5 cm × 1.5 cm) followed by vacuum drying at 120 °C for 24 h. PEDOT:PSS films were dried at 60 °C for 24 h on Teflon plates and then vacuum dried.

Surface Properties. Field-emission scanning electron microscopy (FE-SEM, S-4800, Hitachi) and transmission electron microscopy (TEM, JEM-2010, JEOL) were used for investigating surface and cross-sectional morphologies. Surface species were identified by X-ray photoelectron spectroscopy (XPS; K-alpha spectrometer, Thermo Fisher). Time-of-flight secondary ion mass spectrometry (TOF-SIMS, TOF-SIMS 5, ION TOF, Negative mode) was used with a Bi_3^{2+} gun (50 keV, 0.32 pA).

Bulk Properties. Raman spectra were recorded by a micro-Raman (alpha 300R, WITec) equipped with a He−Ne laser (2 mW, 532 nm). X-ray patterns were obtained by a powder X-ray diffractometer (XRD, D8 ADVANCE A25, BRUKER) with Cu Kα radiation between 10° and 90° at a scan rate of 0.02 degree s^{-1}. Water contents of electrodes vacuum dried at 120 °C were measured by a water contents analyzer (HydroTracer, Aboni). The amounts of PEDOT skin layer on LCO surface were quantified using thermogravimetric analysis (TGA; SDT Q600, TA Instruments). Weight loss due to thermal decomposition of PEDOT in the LCO@PEDOT:PSS was measured at 600 °C at 10 °C min^{-1} under a nitrogen atmosphere. The content of PEDOT:PSS on LCO@3.3Q was estimated at 0.38 wt % of LCO.

Mechanical Properties. Rheological properties of slurries were measured using a rheometer (Haake MARS 3, Thermo Electron). To characterize the binding capability of the PEDOT skin, the 180° peel-off strength of self-standing PEDOT films toward an Al current collector was measured (Autograph AGS-X, SHIMADZU). PEDOT film was laminated with an Al current collector at 160 °C using a roll pressing machine (KP-4500, KIPAE E&T).

Electrochemical Properties. Cell performances such as discharge capacity, C-rate capability, and cyclability were examined using battery test equipment (WBCS-3000 battery cycler, WonAtech). Impedance spectra were obtained over a frequency range from 1 mHz to 1 MHz (VSP classic, Bio-Logic).

RESULTS AND DISCUSSION

Physicochemical Properties of Self-Standing PEDOT:PSS Film. To achieve monocomponent cathodes, the PEDOT skin layer formed on LCO surface should act as a multifunctional thin film showing good electric and ionic conductivities as well as binding capability. First, the basic physicochemical properties of PEDOT:PSS, a key component of LCO@PEDOT:PSS, were investigated with a self-standing PEDOT film (3.3Q, representing the quinoid-type PEDOT:PSS with 3.3 mol of monomeric units of PSS per mole

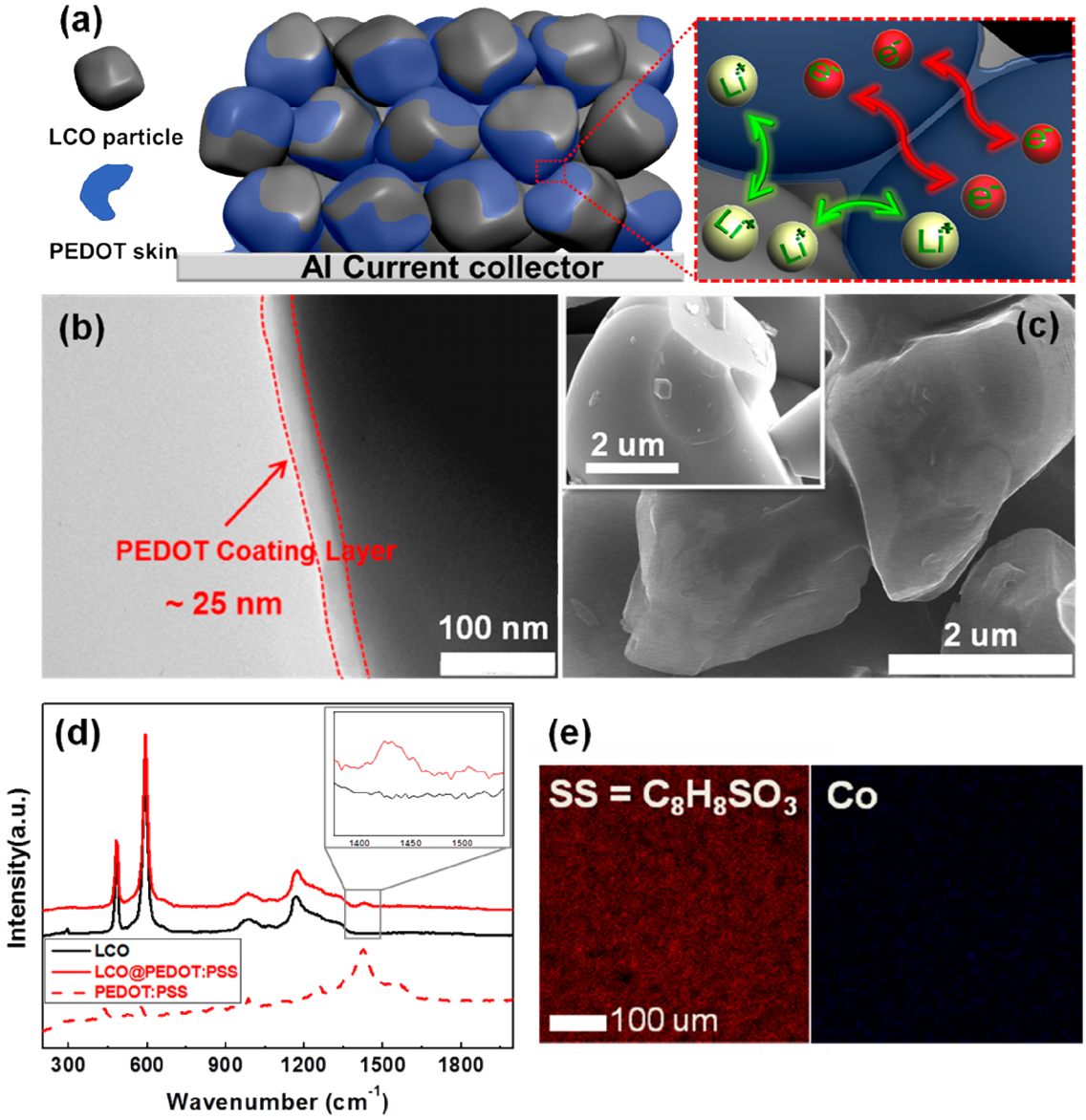

Figure 2. Structural and physicochemical identification of PEDOT:PSS skin layer on LCO. (a) Functions of PEDOT:PSS skin layer as an electrically as well as an ionically conductive binder. (b and c) TEM and SEM images of LCO@PEDOT:PSS. Inset in c shows SEM image of bare LCO. (d) Raman spectra. (e) TOF-SIMS mapping images showing distribution of styrenesulfonate (SS or $C_8H_8SO_3$) and cobalt (Co) on LCO@PEDOT:PSS. 3.3Q was used as PEDOT:PSS.

of PEDOT). Electric conductivity of the PEDOT film was estimated at 392 S cm^{-1} (Figure 1a). The value is high enough for PEDOT to be used as a conductive agent, considering electric conductivities of carbon black (~1000 S cm^{-1})[24] and conventional polymeric binders (electrically inert for polyvinylidene fluoride or PVdF). From the viewpoint of ionic conductivity, PSS dispersed as a dopant in PEDOT:PSS can serve as Li^+-conducting routes, providing polar-solvent-philic environments. The order of magnitude of (lithium) ionic conductivity in PEDOT:PSS was estimated at 10^{-6} S cm^{-1} from impedance data.[25,26] Although PEDOT:PSS may not allow facile lithium-ion transport due to the low ionic conductivity, it can be speculated that the ionic pathways through the nanoscale-thick PEDOT:PSS coating layer at LCO@PEDOT:PSS is too short to slow down the overall kinetics of the electrochemical process. Swelling of the PEDOT:PSS films with carbonate-based electrolyte was traced as a function of time by capacitance parameter T of constant phase element (CPE) measured by electrochemical impedance spectroscopy (Figure 1b). The parameter T is proportional to the interfacial area between electrically conductive material and electrolyte, so that its value is directly related to the degree of swelling. The interfacial area increases at least 15% within 12 h after the impedance signal is stabilized, indicating the film accommodated a considerable amount of electrolyte within their mass. Its swelling kinetics were proven superior to that of PVdF by measuring electrolyte uptake (Figure 1c): time required for reaching saturated uptake = 3 h for PEDOT:PSS versus 10 h for PVdF.

As a parameter to describe the binding capability of the PEDOT:PSS skin layer, the peel-off strength between PEDOT:PSS film and Al current collector was estimated at 1.28 N cm^{-1} (Figure 1d), which is lower than that of PVdF film (= 3.94 N cm^{-1}) currently used in LIBs. The relatively low peel-off strength of PEDOT:PSS film could be explained in terms of the surface energy (indirectly estimated from water

contact angle) difference between the polymer layer and the Al current collector. In comparison to the PEDOT:PSS film (water contact angle ≈ 38.8°), the PVdF film shows a higher water contact angle (81.9°), which seems to be closer to that (110.4°) of the Al current collector (Figure S1, Supporting Information). This result may account for relatively weak interfacial affinity toward the Al current collector. Although the absolute value of peel-off strength of PEDOT:PSS film was found to be relatively low, the PEDOT:PSS skin layer of LCO@PEDOT:PSS enabled successful fabrication of mono-component LCO cathodes with good mechanical flexibility (discussed below).

Structural/Physicochemical Characteristics of LCO@PEDOT:PSS. An important role of a multifunctional PEDOT skin layer, providing electronic/ionic pathways and also binding LCO particles, is schematically illustrated (Figure 2a). A conformal and ultrathin layer of PEDOT:PSS was successfully formed in LCO@PEDOT:PSS by a simple coating process in which LCO was mixed with an aqueous solution of PEDOT:PSS, and then the mixture was filtered. The surface of LCO particles is covered with a 25 nm thick PEDOT:PSS layer, showing smooth edges at the boundaries of faces (Figure 2b and 2c), in contrast to the sharp edges of bare LCO (inset of Figure 2c). Notably, this ultraskinny PEDOT:PSS layer formed on the LCO surface is a salient structural feature. Many previous studies on PEDOT:PSS for battery applications were mainly focused on the use of PEDOT:PSS as a conductive coating layer of electrode active materials or an organic-based electrode active material combined with lithium metal oxides.[11,12,20,21] The thickness of the PEDOT:PSS skin layer is expected to be affected by the PEDOT:PSS concentration in the coating solution and also processing parameters such as filtration method, time, and so forth. Further works to examine the effect of the solution concentration and processing variables on the skin layer thickness, which are expected to exert a significant influence on the electrochemical properties of resulting electrodes, will be conducted in future studies. The chemical materiality of the PEDOT:PSS skin layer on the surface of LCO was identified by the characteristic peaks of the thiophene rings in the Raman spectra (Figure 2d).[27,28] Comparison of XRD patterns between bare LCO and LCO@PEDOT:PSS confirmed that introduction of PEDOT:PSS does not disrupt the crystalline structure of LCO (Figure S2a, Supporting Information). LCO@PEDOT:PSS was a typical layered structure of hexagonal α-$NaFeO_2$ type with $R\bar{3}m$ space group.[29,30]

Uniformity of the PEDOT:PSS skin layer on the LCO surface was confirmed by TOF-SIMS mapping images (Figure 2e). Styrenesulfonate fractions ($C_8H_8SO_3$, indicated by red dots) of PEDOT:PSS were uniformly dispersed over a wide area of LCO surface. Strong intensities of Co elements were not detected, indicating that the LCO surface is well shielded with the PEDOT:PSS layer. The amount of PEDOT:PSS skin loaded on LCO was estimated at less than 0.4% (wt/wt) by thermogravimetric analysis (TGA, Figure S2b, Supporting Information).[31] The PEDOT:PSS amount can be controlled by tuning the mixing composition of LCO in PEDOT:PSS solution. LCO@PEDOT:PSS powders with less than the 0.4% PEDOT:PSS contents (0.2% in Figure 3a) showed poor adhesion ability on current collectors, so that the LCO@PEDOT:PSS powders with 0.4% PEDOT:PSS content were used as a representative sample.

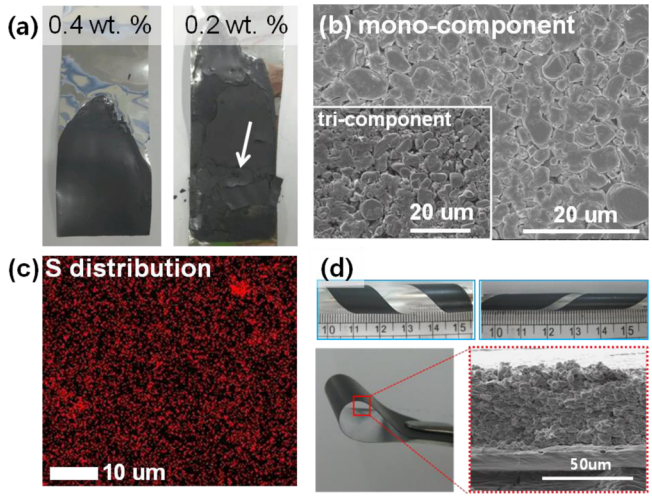

Figure 3. Monocomponent electrodes based on LCO@PEDOT:PSS. (a) LCO@PEDOT:PSS coated on Al foils with different PEDOT:PSS contents. (b) Cross-sectional FE-SEM image (inset: a conventional tricomponent electrode). (c) Sulfur (S) distribution measured by EDS. (d) Rolling a monocomponent electrode (including current collector) around glass rods of 5 and 10 mm and folding. Cross-sectional FE-SEM image on the curved part of the folded electrode. 3.3Q was used as a PEDOT:PSS.

Processability of Monocomponent Electrode Fabrication. The monocomponent cathode comprising solely LCO@PEDOT:PSS powders on top of an Al current collector was successfully fabricated (Figure S3 and Movie S1, Supporting Information). From the viewpoint of the electrode manufacturing process, only a single component (LCO@PEDOT:PSS) was dispersed in a solvent for making electrode slurry without additional binders and conductive agents. Moreover, water was used as dispersion solvent, providing environmentally benign benefits. In a conventional process, both binders (PVdF) and conductive agents (carbon black) are introduced into an organic solvent such as NMP with electrode active materials, leading to tricomponent electrode systems. Our monocomponent slurry (LCO@PEDOT:PSS in water) behaved rheologically appropriate for being coated using currently available coating machines. Similar to the conventional tricomponent ones, the LCO@PEDOT:PSS slurry presented a non-Newtonian response (i.e., shear-thinning behavior[32,33]) (Figure S4, Supporting Information). This result shows that LCO@PEDOT:PSS coating on current collectors can be achieved without suffering from serious processing difficulties, although less viscous fluidity is observed at a fixed shear rate. In multicomponent slurries, there is every possibility that nonuniform dispersions in solvents and coating films are caused by incompatibility in dispersion solvents and a difference of rheological properties between components, respectively. However, monocomponent systems would not experience such problems only if rheological requirements of the component were met.

There were no significant differences observed between the monocomponent cathode and the conventional tricomponent cathode in terms of coating uniformity and adhesion capability (Figure S4, Supporting Information, and Figure 3b and 3c). LCO@PEDOT:PSS powders were closely packed and interconnected to each other. The highly developed interstitial voids formed between the LCO@PEDOT:PSS powders are expected to offer ionic transport channels that allow facile

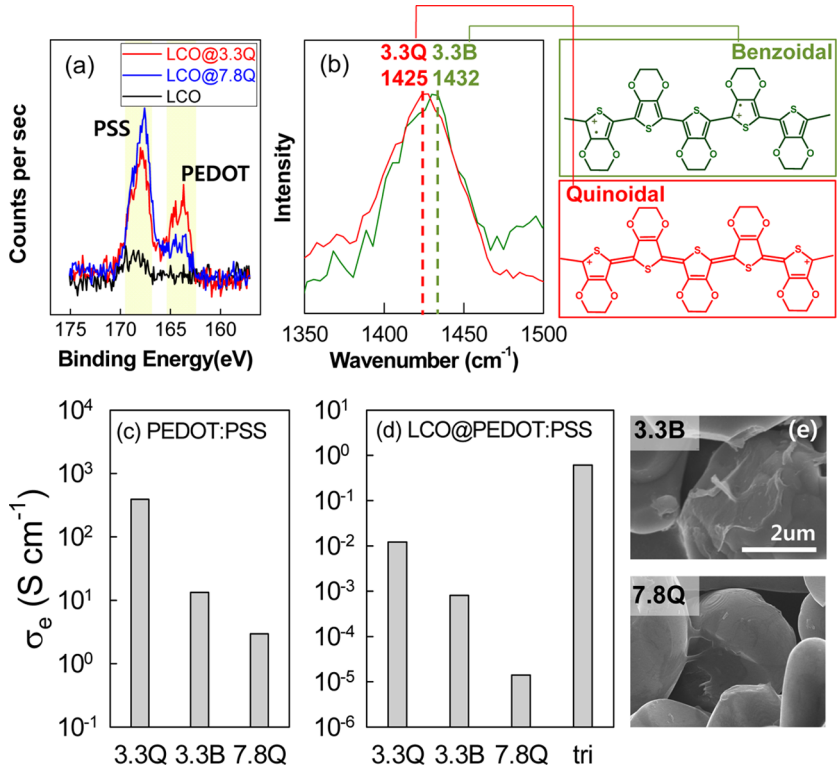

Figure 4. Composition and conformation effects of PEDOT:PSS skin on electric conductivities of LCO@PEDOT:PSS. (a) X-ray photoelectron spectra (XPS) depending on PSS contents of PEDOT:PSS skins (X_{PSS}). Arabic numbers of 3.3Q and 7.8Q indicate molar ratios of PSS to PEDOT (X_{PSS}). (b) Raman spectra of two different structural conformations of PEDOT:PSS. Q = quinoidal; B = benzoidal. (c and d) Electric conductivities of films and LCO@PEDOT:PSS, respectively. (e) FE-SEM images of 3.3B and 7.8Q on LCO.

accessibility of liquid electrolyte to LCO surface. To check the physical integrity and flexibility of the monocomponent cathode, their morphological changes were investigated after exposure to mechanical deformation. Neither significant physical breakage nor dimensional failure was observed after both rolling around glass rods (diameter = 5 and 10 mm) and folding, indicating good physical integrity in terms of adhesion and cohesion (Figure 3d).

To clarify concerns associated with residual water in electrodes, the water contents were compared between our monocomponent cathode (aqueous-dispersion-based) and the conventional electrode (NMP-dispersion-based) (Figure S5, Supporting Information). The water content in the monocomponent electrode was estimated at the same order of magnitude but a higher value compared with that of the conventional composite electrode. However, the difference of residual water contents did not impair electrochemical performances seriously in this work even if it should be minimized to suppress water-induced side reactions.

Effect of PEDOT:PSS Skin Layer as a Function of PSS Content and Structural Conformation of PEDOT. In our monocomponent electrodes, electric conduction is significantly affected by the PEDOT:PSS skin layer. Electric conductivity of PEDOT:PSS was tuned by PSS contents and its conformation of polymeric chain. Two kinds of PEDOT:PSS were used in terms of the molar ratio of PSS to PEDOT (X_{PSS} = 3.3 and 7.8, calculated from the manufacturer's specification). The ratios of the polymers were consistently reflected in their coating skins on LCO, which were estimated by the area ratios of the peak at ~167.7 eV (assigned to PSS) to the peak at ~164 eV (assigned to PEDOT) in X-ray photoelectron spectra (XPS) of LCO@PEDOT:PSS (Figure 4a).[34] PEDOT has positive charges every several (3−4) monomeric units along polymeric backbone.[34,35] The positively charged ensembles work as a charge carrier for electric conduction. In its conductive state, therefore, the counteranions referred to as dopants should be introduced into PEDOT to neutralize its positive charges. PSS acts as a polyanionic dopant in PEDOT:PSS. An extra amount of PSS is used not as a dopant but just as an insulating mass to hinder the electric pathway (3.3Q versus 7.8Q in Figure 4c, where the Arabic number = X_{PSS} and Q = Quinoid). Also, the extra PSS enables PEDOT to be dispersed in water even if the polymer (PEDOT) is not soluble in aqueous solutions. On the basis of the assumption that every three monomeric units has one positive charge (X_{PSS} = 3), most of the sulfonates of PSS in 3.3Q are used as a dopant while more than 50% of the sulfonates of 7.8Q is not helpful in terms of conductivity.

As the second factor controlling the electric conductivity of PEDOT:PSS, the conformation of the polymer structure was tuned. Solvent (dimethyl sulfoxide or DMSO here) annealing induced a conformational transformation from a benzoid-favoring coil structure (characterized by the peak at 1432 cm^{-1} in Raman spectra of Figure 4b) to a quinoid-favoring linear or extended coil structure (1425 cm^{-1}), enhancing the electric conductivity (3.3Q versus 3.3B in Figure 4c where B = Benzoid).[36−38] The conductivities of PEDOT:PSS films were reflected on LCO@PEDOT:PSS (Figure 4c and 4d), even if no appreciable difference in the surface morphology was observed between all LCO@PEDOT:PSS (SEM images in Figure 2c for 3.3Q and Figure 4e for 3.3B and 7.8Q; electrode photos in Figure 3a left for 3.3Q and Figure S6, Supporting Information, for 3.3B and 7.8Q). However, they did not surpass the

conductivity of the tricomponent composite electrode based on carbon black conductive additives.

Cell Performances of Monocomponent Cathodes. Cell performances of the monocomponent cathodes were investigated versus the conventional tricomponent electrode at various charge/discharge conditions, with particular focus on variation of their electric conductivity. The monocomponent electrodes with highly conductive PEDOT:PSS (3.3Q and 3.3B; Not 7.8Q) delivered slightly higher volumetric capacities than the tricomponent counterpart in terms of cycle retention and rate capability (Figure 5a–c), even if electric conductivities

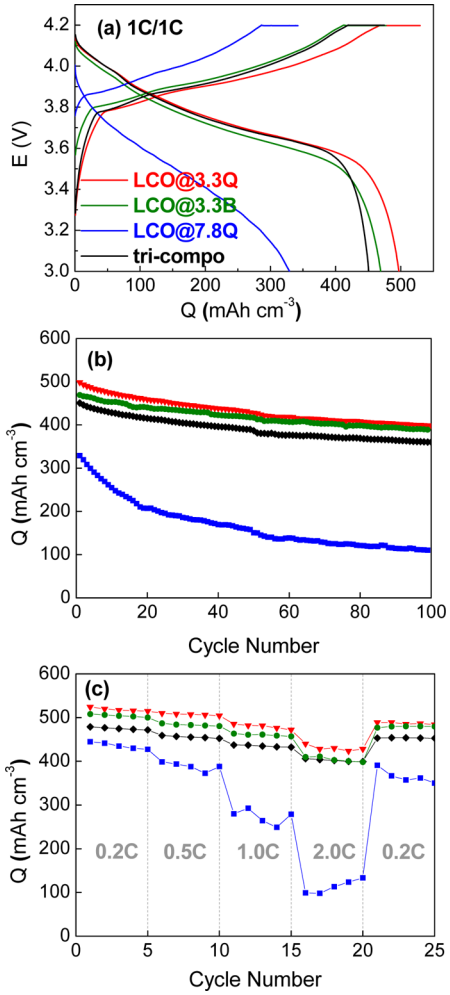

Figure 5. Cell performance of the monocomponent cathode versus the tricomponent counterpart. (a) Potential profiles during charge and discharge at 1 C. (b) Capacity retention during cycling (charge/discharge rate =1.0 C/1.0 C). (c) C-rate dependency of discharge capacities. Charge rate was fixed at 0.2 C, while discharge rates were varied as indicated.

of the monocomponent electrodes are lower than that of the three-component counterpart (Figure 4 d). This capacity gain may arise from the higher density of active materials in electrodes even with the same thickness because neither additional binders nor conductive agents were used (Table 1). Only the PEDOT:PSS skin layer of LCO@PEDOT:PSS plays a role as a conductive pathway. The initial volumetric discharge capacity of a monocomponent electrode (LCO@3.3Q) was estimated at 497 mAh cm^{-3} at 1.0 C discharge following 1.0 C charge, demonstrating a 10% increase from that of the tricomponent control (Figure 5a). Long-term electrochemical and structural stability of the monocomponent cathodes were also verified by their cycle retention similar to the tricomponent control (Figure 5b), and no detectable level of morphological disruption was observed after the 100th cycle (Figure 6a), respectively. Cell impedances were considerably developed after 100 cycles with less conductive PEDOT:PSS (Figure 6b). The most conductive 3.3Q led to comparatively small growth of impedance or charge transfer resistance (R_{CT}): the difference between before and after cycling (ΔR_{CT}) = 25 ohm for 3.3Q versus 60 ohm for 3.3B and 300 ohm for 7.8Q.

Whether conductivity is a capacity-liming factor or not should be determined by how fast energy is extracted (Figure 5c). Specific capacities per active material mass (neither volumetric capacity mentioned above nor capacities per total electrode mass) were found at similar values between the monocomponent electrodes with LCO@3.3Q or 3.3B and the tricomponent one until 1.0 C (Figure S7, Supporting Information). At 2.0 C, however, the electrode based on less conductive 3.3B PEDOT:PSS coating (~10° mS cm^{-1}) delivered less capacity per active mass. It means that the conductivity level does not limit an intrinsic capacity of active mass at least until 2.0 C only if it is higher than ~10^{1} mS cm^{-1} (for the monocomponent electrode with LCO@3.3Q; cf. ~600 mS cm^{-1} for the tricomponent). The lowest conductive coating by 7.8Q (~10^{-2} mS cm^{-1}) showed the most inferior performances at all C rates from 0.2 C.

Eliminating binders and conductive agents in the monocomponent electrodes enabled high-density electrodes affording a high volumetric energy density of cells. Electrode densities (d_{Ed}) of the above experiments were 3.41 and 3.56 g cm^{-3} for monocomponent and tricomponent electrodes, respectively (Table 1). From the electrode density results, the loading density of LCO active materials themselves (d_{LCO}) was estimated. The comparison of d_{LCO} between the two electrodes shows that the monocomponent electrode presents a higher value than the tricomponent one, demonstrating the denser packing of LCO powders at the monocomponent electrode. Meanwhile, it is difficult to obtain high loading density electrode guaranteeing reliable cell performances with conventional electrode compositions, because electric and ionic conductions tend to be traded off with increasing electrode loading density. At a high loading density of tricomponent electrodes, conductive agents are more closely packed into an enhanced percolation configuration, improving electric conductivity. Simultaneously, the space sitting between particles (corresponding to electrode porosity) is reduced with increasing electrode loading density (Table 1), thus causing some concerns on electrolyte accessibility inside the electrodes. By comparison, for the monocomponent electrodes based on LCO@PEDOT:PSS, the electrode porosity was not seriously decreased (porosity ≈ 17.1% in Table 1) as the PEDOT:PSS skin layer acts not only as an electric conductor but also as an ionic conductor.

To confirm the advantageous effect of LCO@PEDOT:PSS at high density loading conditions, the monocomponent and tricomponent electrodes were compared at a similar loading density value (d_{Ed} ≈ 5.02 (for tricomponent cathode), 4.91 g cm^{-3} (for monocomponent cathode)). Both electrodes show the dense packing of electrode components (Figure 7a and 7b); however, their electrode porosities were found to be different (Table 1). Due to the presence of PEDOT:PSS skin layer, which was well distributed in the through-thickness direction of

Table 1. Compositions and Densities of Monocomponent and Tricomponent Electrodes

	thickness (μm), average value [min−max]	d_{Ed} electrode density (g cm^{-3}), average value [min−max]	d_{LCO} loading density (g cm^{-3}), average value [min−max]	porosity (%), average value [min−max]
low-density loading				
tri[a]	50 [49−52]	3.56 [3.50−3.67]	3.38 [3.33−3.49]	24.2 [21.9−25.3]
mono[a]	50 [49−51]	3.41 [3.37−3.45]	3.41 [3.37−3.45]	33.1 [32.4−33.7]
high-density loading				
tri[a]	55 [52−57]	5.02 [4.98−5.08]	4.77 [4.73−4.83]	8.2 [7.4−9.5]
mono[a]	55 [53−57]	4.91 [4.89−4.93]	4.91 [4.89−4.93]	17.1 [15.5−18.1]

[a]Tri = tricomponent electrodes consisting of LCO, PVdF, and carbon black at 95:3:2 by weight. Mono = monocomponent electrodes consisting of only LCO@PEDOT:PSS; 3.3Q was used as a PEDOT:PSS for the high-density loading electrodes.

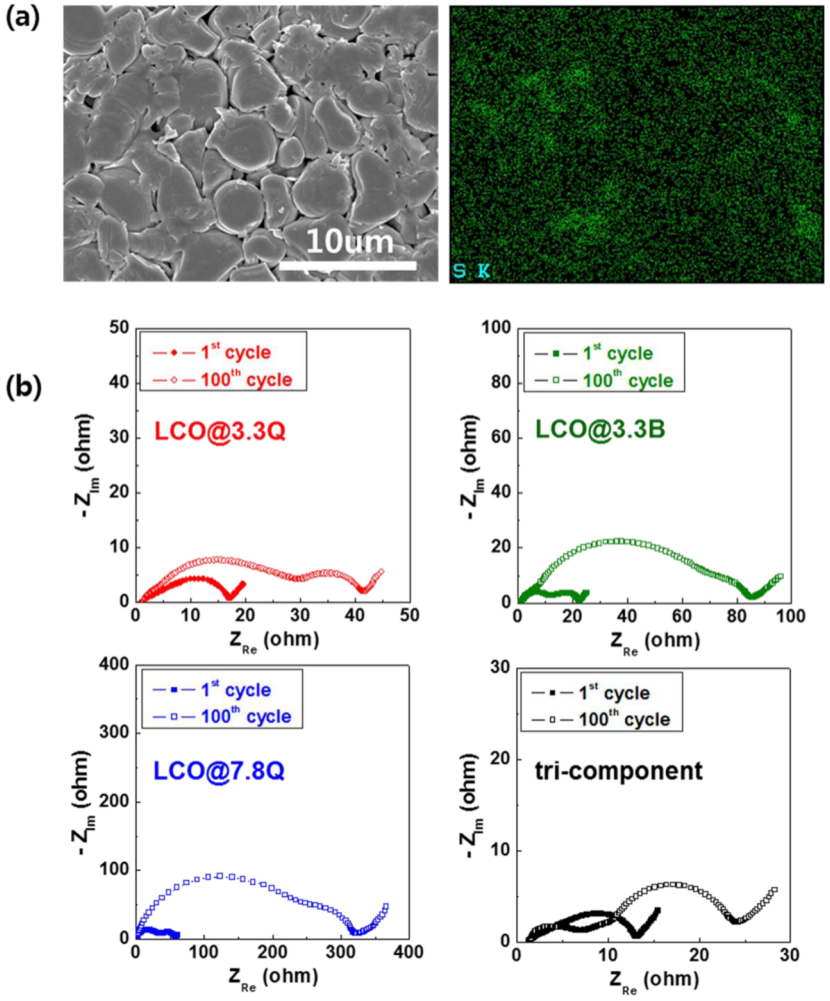

Figure 6. Long-term structural and electrochemical stability of the monocomponent electrode after 100th cycle. (a) Morphology by FE-SEM and sulfur (S) map in the same scale by EDS. 3.3Q was used as PEDOT:PSS. (b) Impedance spectra obtained before and after 100th cycling.

the monocomponent cathode (from the inset image of Figure 7a showing sulfur elements), the monocomponent cathode presented higher electrode porosity (~17.1%) than the tricomponent cathode (~8.2%), which may thus contribute to facilitating electrolyte accessibility. The capacity retention during charge/discharge cycling clearly exhibited the benefit of the PEDOT:PSS skin layer as an electronically/ionically conductive film (Figure 7c and 7d): 81% for the monocomponent electrode versus less than 50% for the tricomponent control at the 150th cycle. Therefore, use of PEDOT:PSS skin layer on active materials can be suggested as a technological breakthrough to overcome a deadlock on developing high-density electrodes.

CONCLUSION

In summary, a new class of monocomponent LCO cathode without additional binders and conductive agents was successfully fabricated using solely LCO powders wrapped with ultrathin layers of conducting polymer (PEDOT:PSS). The PEDOT:PSS skin on the LCO surface showed unusual multifunctionality as an alternative binder as well as mixed ionic/electronic conduction layer. The electric conductivity of monocomponent LCO cathode was controlled by changing the PSS content and also the structural conformation (benzoid-favoring and quinoid-favoring) of PEDOT in the PEDOT:PSS skin layer. Elimination of nonelectroactive components such as

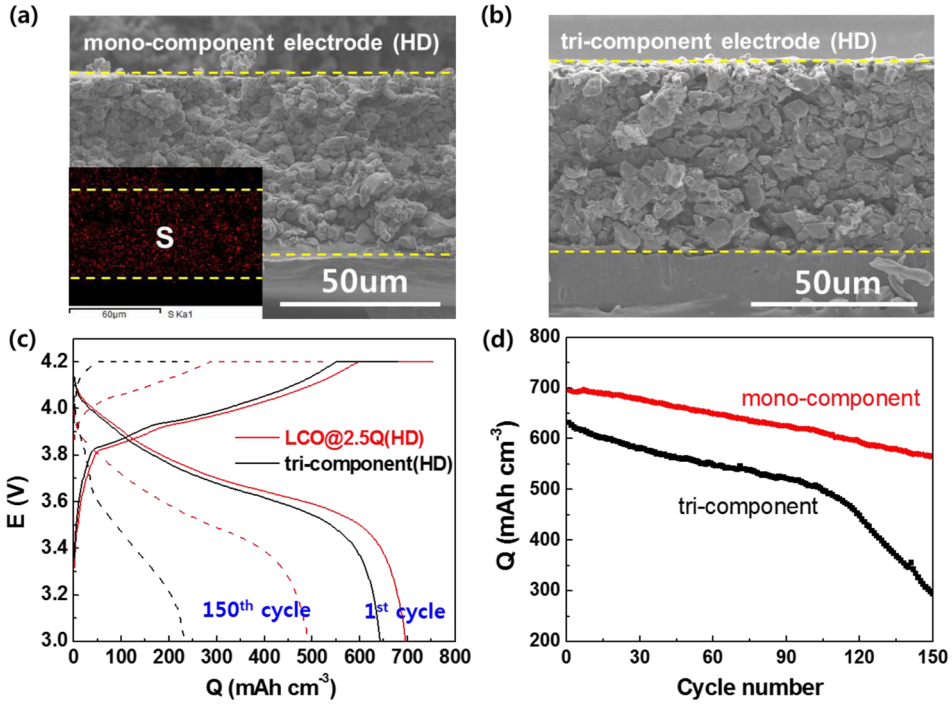

Figure 7. Structural and electrochemical characterization of high-density (HD) cathodes (loading density (d_{Ed}) ≈ 5 g cm^{-3}). (a) Cross-sectional morphology of the HD monocomponent electrode based on LCO@3.3Q by FE-SEM (inset is an EDS image showing the distribution of sulfur (S) element). (b) Cross-sectional morphology of the HD tricomponent electrode by FE-SEM. (c) Potential profiles of charge and discharge at the 1st and 150th cycle. (d) Capacity retention of high-density electrodes during cycling. Cells were charged and then discharged at 1.0 C.

binders and conductive agents enabled the higher energy density monocomponent LCO cathode. Moreover, the high mass loading density of the LCO cathode was realized with the PEDOT:PSS skin layer without impairing electrochemical performance. We believe that the PEDOT:PSS skin strategy can be suggested as a platform technology applicable to a wide variety of electrode active materials without the need of modifying pre-established electrode manufacturing processes.

■ ASSOCIATED CONTENT

Ⓢ Supporting Information

XRD, TGA of LCO@PEDOT:PSS, and viscosity of the monocomponent and tricomponent slurry, and residual water contents in cathode electrode, surface morphology of the monocomponent cathodes based on two different PEDOT:PSS, C-rate dependency of discharge capacities per active mass. This material is available free of charge via the Internet at http://pubs.acs.org.

■ AUTHOR INFORMATION

Corresponding Authors

*Phone: +82-52-217-2512. Fax +82-52-217-2019. E-mail: philiphobi@hotmail.com.

*Phone: +82-52-217-2948. Fax +82-52-217-2019. E-mail: syleek@unist.ac.kr.

Author Contributions

J.-M.K. and H.-S.P. contributed equally to this work.

Notes

The authors declare no competing financial interest.

■ ACKNOWLEDGMENTS

This research was supported by MOTIE (Star: 20135020900030), MSIP (C-ITRC: NIPA-2013-H0301-13-1009), and MOE (NRF-2009-C1AAA001-2009-0093307). This work was also supported by the BK21 Plus Program (META-material-based Energy Harvest and Storage Technologies, 10Z20130011057) funded by the Ministry of Education (MOE, Korea) and National Research Foundation of Korea (NRF).

■ REFERENCES

(1) Cheng, F.; Liang, J.; Tao, Z.; Chen, J. Functional Materials for Rechargeable Batteries. *Adv. Mater.* **2011**, *23*, 1695−1715.

(2) Liu, C.; Li, F.; Ma, L. P.; Cheng, H. M. Advanced Materials for Energy Storage. *Adv. Mater.* **2010**, *22*, E28−E62.

(3) Tarascon, J.-M.; Armand, M. Issues and Challenges Facing Rechargeable Lithium Batteries. *Nature* **2001**, *414*, 359−367.

(4) Manthiram, A. Materials Challenges and Opportunities of Lithium Ion Batteries. *J. Phys. Chem. Lett.* **2011**, *2*, 373−373.

(5) Whittingham, M. S. Lithium Batteries and Cathode Materials. *Chem. Rev.* **2004**, *104*, 4271−4302.

(6) Bruce, P. G.; Scrosati, B.; Tarascon, J. M. Nanomaterials for Rechargeable Lithium Batteries. *Angew. Chem., Int. Ed.* **2008**, *47*, 2930−2946.

(7) Guo, Y. G.; Hu, J. S.; Wan, L. J. Nanostructured Materials for Electrochemical Energy conversion and storage devices. *Adv. Mater.* **2008**, *20*, 2878−2887.

(8) Luo, S.; Wang, K.; Wang, J.; Jiang, K.; Li, Q.; Fan, S. Binder Free $LiCoO_2$/Carbon Nanotube Cathodes for High Performance Lithium Ion Batteries. *Adv. Mater.* **2012**, *24*, 2294−2298.

(9) Sun, Y.; Wang, J.; Zhao, B.; Cai, R.; Ran, R.; Shao, Z. Binder-Free α-MoO_3 Nanobelt Electrode for Lithium-Ion Batteries Utilizing Van Der Waals Forces for Film Formation and Connection with Current Collector. *J. Mater. Chem. A* **2013**, *1*, 4736−4746.

(10) Ban, C.; Wu, Z.; Gillaspie, D. T.; Chen, L.; Yan, Y.; Blackburn, J. L.; Dillon, A. C. Nanostructured $Fe3O_4$/SWNT Electrode: Binder Free and High Rate Li Ion Anode. *Adv. Mater.* **2010**, *22*, E145−E149.

(11) Huang, Y.-H.; Goodenough, J. B. High-rate $LiFePO_4$ Lithium Rechargeable Battery Promoted by Electrochemically Active Polymers. *Chem. Mater.* **2008**, *20*, 7237−7241.
(12) Trinh, N.; Saulnier, M.; Lepage, D.; Schougaard, S. Conductive Polymer Film Supporting $LiFePO_4$ as Composite Cathode for Lithium Ion Batteries. *J. Power Sources* **2012**, *221*, 284−289.
(13) Liu, G.; Xun, S.; Vukmirovic, N.; Song, X.; Olalde Velasco, P.; Zheng, H.; Battaglia, V. S.; Wang, L.; Yang, W. Polymers with Tailored Electronic Structure for High Capacity Lithium Battery Electrodes. *Adv. Mater.* **2011**, *23*, 4679−4683.
(14) Yao, Y.; Liu, N.; McDowell, M. T.; Pasta, M.; Cui, Y. Improving The Cycling Stability of Silicon Nanowire Anodes with Conducting Polymer Coatings. *Energy Environ. Sci.* **2012**, *5*, 7927−7930.
(15) Lee, S. H.; Kim, Y. H.; Deshpande, R.; Parilla, P. A.; Whitney, E.; Gillaspie, D. T.; Jones, K. M.; Mahan, A.; Zhang, S.; Dillon, A. C. Reversible Lithium Ion Insertion in Molybdenum Oxide Nanoparticles. *Adv. Mater.* **2008**, *20*, 3627−3632.
(16) Ha, D.-H.; Islam, M. A.; Robinson, R. D. Binder-Free and Carbon-Free Nanoparticle Batteries: A Method for Nanoparticle Electrodes without Polymeric Binders or Carbon Black. *Nano Lett.* **2012**, *12*, 5122−5130.
(17) Abouimrane, A.; Compton, O. C.; Amine, K.; Nguyen, S. T. Non-Annealed Graphene Paper as a Binder-Free Anode for Lithium-Ion Batteries. *J. Phys. Chem. C* **2010**, *114*, 12800−12804.
(18) Gwon, H.; Kim, H. S.; Lee, K. U.; Seo, D. H.; Park, Y. C.; Lee, Y. S.; Ahn, B. T.; Kang, K. Flexible Energy Storage Devices Based on Graphene Paper. *Energy Environ. Sci.* **2011**, *4*, 1277−1283.
(19) Hwang, T. H.; Lee, Y. M.; Kong, B. S.; Seo, J. S.; Choi, J. W. Electrospun Core-Shell Fibers for Robust Silicon Nanoparticle-Based Lithium Ion Battery Anodes. *Nano Lett.* **2012**, *12*, 802−807.
(20) Arbizzani, C.; Mastragostino, M.; Rossi, M. Preparation and Electrochemical Characterization of a Polymer $Li_{1.03}Mn_{1.97}O_4$/PEDOT Composite Electrode. *Electrochem. Commun.* **2002**, *4*, 545−549.
(21) Wang, G.; Yang, L.; Chen, Y.; Wang, J.; Bewlay, S.; Liu, H. An Investigation of Polypyrrole-$LiFePO_4$ Composite Cathode Materials for Lithium-Ion Batteries. *Electrochim. Acta* **2005**, *50*, 4649−4654.
(22) Park, K. S.; Schougaard, S. B.; Goodenough, J. B. Conducting Polymer/Iron Redox Couple Composite Cathodes for Lithium Secondary Batteries. *Adv. Mater.* **2007**, *19*, 848−851.
(23) Boyano, I.; Blazquez, J. A.; de Meatza, I.; Bengoechea, M.; Miguel, O.; Grande, H.; Huang, Y.; Goodenough, J. B. Preparation of C-$LiFePO_4$/Polypyrrole Lithium Rechargeable Cathode by Consecutive Potential Steps Electrodeposition. *J. Power Sources* **2010**, *195*, 5351−5359.
(24) Marinho, B.; Ghislandi, M.; Tkalya, E.; Koning, C. E. Electrical Conductivity of Compacts of Graphene, Multi-Wall Carbon Nanotubes, Carbon Black, and Graphite Powder. *Powder Technol.* **2012**, *221*, 351−358.
(25) Guangchun, L.; Peter, G. P. Ion Transport in Poly-(3,4Ethylenedioxythiophene) . Poly(Styrene-4-Sulfonate) Composites. *Phys. Chem. Chem. Phys.* **2000**, *2*, 1255−1260.
(26) Catia, A.; Maurizio, B.; Elisa, M.; Marina, M. Methanol oxidation by PEDOT-pSS/PtRu in DMFC. *J. Power Sources* **2008**, *178*, 584−590.
(27) Ouyang, J.; Chu, C. W.; Chen, F. C.; Xu, Q.; Yang, Y. Polymer Optoelectronic Devices with High Conductivity Poly (3,4 Ethylenedioxythiophene) Anodes. *J. Macromol. Sci., Part A: Pure Appl. Chem.* **2004**, *41*, 1497−1511.
(28) Tung, V. C.; Kim, J.; Cote, L. J.; Huang, J. Sticky Interconnect for Solution-Processed Tandem Solar Cells. *J. Am. Chem. Soc.* **2011**, *133*, 9262−9265.
(29) Kushida, K.; Kuriyama, K. Sol-Gel Growth of $LiCoO_2$ Films on Si Substrates by a Spin-Coating Method. *J. Cryst. Growth* **2002**, *237*, 612−615.
(30) Sun, Y.-K.; Cho, S.-W.; Myung, S.-T.; Amine, K.; Prakash, J. Effect of AlF_3 Coating Amount on High Voltage Cycling Performance of $LiCoO_2$. *Electrochim. Acta* **2007**, *53*, 1013−1019.
(31) Sun, D. C.; Sun, D. S. The Synthesis and Characterization of Electrical and Magnetic Nanocomposite: PEDOT/PSS-Fe_3O_4. *Mater. Chem. Phys.* **2009**, *118*, 288−292.
(32) Lee, G.-W.; Ryu, J. H.; Han, W.; Ahn, K. H.; Oh, S. M. Effect of Slurry Preparation Process on Electrochemical Performances of $LiCoO_2$ Composite Electrode. *J. Power Sources* **2010**, *195*, 6049−6054.
(33) Li, C.-C.; Lee, J.-T.; Lo, C.-Y.; Wu, M.-S. Effects of PAA-NH_4 Addition on The Dispersion Property of Aqueous $LiCoO_2$ Slurries and The Cell Performance of As-Prepared $LiCoO_2$ Cathodes. *Electrochem. Solid-State Lett.* **2005**, *8*, A509−A512.
(34) Park, H.-S.; Ko, S.-J.; Park, J.-S.; Kim, J. Y.; Song, H.-K. Redox-Active Charge Carriers of Conducting Polymers as a Tuner of Conductivity and its Potential Window. *Sci. Rep.* **2013**, *3*, 976−983.
(35) Zotti, G.; Zecchin, S.; Schiavon, G.; Louwet, F.; Groenendaal, L.; Crispin, X.; Osikowicz, W.; Salaneck, W.; Fahlman, M. Electrochemical and XPS Studies Toward The Role of Monomeric and Polymeric Sulfonate Counterions in the Synthesis, Composition, and Properties of Poly (3, 4-Ethylenedioxythiophene). *Macromolecules* **2003**, *36*, 3337−3344.
(36) Na, S.-I.; Wang, G.; Kim, S.-S.; Kim, T.-W.; Oh, S.-H.; Yu, B.-K.; Lee, T.; Kim, D.-Y. Evolution of Nanomorphology and Anisotropic Conductivity in Solvent-Modified PEDOT: PSS Films for Polymeric Anodes of Polymer Solar Cells. *J. Mater. Chem.* **2009**, *19*, 9045−9053.
(37) Kim, Y. H.; Sachse, C.; Machala, M. L.; May, C.; Muller Meskamp, L.; Leo, K. Highly Conductive PEDOT: PSS Electrode with Optimized Solvent and Thermal Post Treatment for ITO Free Organic Solar Cells. *Adv. Funct. Mater.* **2011**, *21*, 1076−1081.
(38) Stocker, T.; Kohler, A.; Moos, R. Why Does The Electrical Conductivity in PEDOT: PSS Decrease with PSS Content? A Study Combining Thermoelectric Measurements with Impedance Spectroscopy. *J. Polym. Sci., Part B: Polym. Phys.* **2012**, *50*, 976−983.